Hematitic concretions at Meridiani Planum, Mars: Their growth timescale and possible relationship with iron sulfates

Elliot Sefton-Nash *, David C. Catling

Department of Earth Sciences, University of Bristol, Queens Road, Bristol, BS8 1RJ, UK

Abstract

Using diffusion-based models for concretion growth, we calculate growth times of hematitic concretions that have been found in the Burns formation at Meridiani Planum, Mars, by NASA's Opportunity Mars Exploration Rover. Growth times of ~350–1900 terrestrial years are obtained for the observed size range of the concretions over a range of parameters representing likely diagenetic conditions and allowing for an iron source from diagenetic redistribution. This time scale is consistent with radiometric age constraints for the growth time of iron oxide concretions in sandy sediments of the acid-saline Lake Brown in Western Australia (<3000 yr) reported elsewhere. We consider the source of the iron for Meridiani concretions by calculating the constraints on the supply of Fe^{3+} to growing concretions from the dissolution and oxidation rates of iron minerals on early Mars. Mass balance arguments suggest that acid dissolution of jarosite $((H_3O,K)(Fe^{3+}3(OH)_6(SO_4)_2))$ and minor ferric sulfates is probably the most plausible dominant contributor to Fe^{3+} in the concretions. Ferrous iron released from melanterite $(Fe^{2+}SO_4 \cdot 7H_2O)$ that is subsequently oxidized could also have been an important iron source if melanterite existed prior to diagenesis. Our conclusion that the iron is sourced from iron sulfates may explain the global observation from orbiters that grey crystalline hematite occurs in association with sulfate deposits.
© 2008 Elsevier B.V. All rights reserved.

Keywords: Mars; concretions; sulfates; Meridiani; hematite

1. Introduction

Since 2004, NASA's Mars Exploration Rovers have yielded unprecedented data on Martian surface geology and chemistry. In Meridiani Planum, the Opportunity rover has examined a series of outcrops that form a stratigraphic unit, which was named the Burns Formation. The Burns formation is at least 800 m thick (Edgett, 2005) and its analysis reveals a sulfate-rich dune–interdune-playa sedimentary sequence (Grotzinger et al., 2005; McLennan et al., 2005) populated by 2–5 mm hematitic (Fe_2O_3) spherules (Squyres and Athena Science, 2004). In a wider context, massive accumulations of sulfates have also been remotely detected from the OMEGA (Observatoire pour la Minéralogie, l'Eau, les Glaces, et l'Activité) instrument on ESA's Mars Express (Gendrin et al., 2005) and the CRISM (Compact Reconnaissance Imaging Spectrometer for Mars) instrument on NASA's Mars Reconnaissance Orbiter (Knudson et al., 2007). Some of these sulfates are associated with hematite, such as in Aram Chaos (Bibring et al., 2007; Glotch and Christensen, 2005), so determining the genetic relationship between sulfates and hematite is an important issue for understanding some of the most interesting geology of Mars.

Several origins have been suggested for the hematite spherules, but there is strong sedimentological evidence that they are concretions, which form when water carries dissolved minerals through sediments or porous rocks and minerals precipitate concentrically and incorporate or replace surrounding sediments (although the Meridiani concretions do not show morphological or compositional nuclei). Knauth et al. (2005) suggested that the spherules are volcanic or impact-induced lapilli. However, the

---

* Corresponding author. Tel.: +44 117 331 5196; fax: +44 117 925 3385.
E-mail address: e.sefton-nash@bristol.ac.uk (E. Sefton-Nash).

sedimentology clearly favours a concretionary origin: 1) laminae are not deflected around the spherules by burial or compaction, so they likely crystallized on the spot, unlike the case of drops of molten lava (glass spherules) or pellets of congealed ash (lapilli) 2) spherules show banding or grooves that parallel the surrounding laminations, as expected for concretions 3) spherules are distributed uniformly throughout the unit rather than in bedding planes, 4) a distinct Fe-rich mineralogy is inconsistent with volcanic lapilli or impact glasses and 5) doublets are present, which are statistically unlikely for lapilli but expected for concretions (Squyres et al., 2004; McLennan et al., 2005). Thus, the consensus view is that hematite spherules formed as concretions when iron-rich groundwater penetrated the stratigraphic column.

Different terrestrial analogues have been proposed for the hematite spherules. Morris et al. (2005) suggested a hydrothermal origin through acid-sulfate alteration of basaltic tephra, using the analogy of spherules observed at the Mauna Kea volcano, Hawaii. These 10–100 micron-sized spherules are compositionally zoned. However, the Meridiani spherules are larger and apparently of homogeneous composition, suggesting they were formed in less fluids and over longer timescales. Chan et al. (2004) compare concretions in Utah's Navajo Sandstone, which formed in porous quartz arenite from the dissolution of iron oxides by reducing fluids and subsequent Fe-precipitation. The variety of concretions illustrated in the Navajo sandstone establishes important geometries and distribution relationships. However, there are notable chemical differences between these and Meridiani concretions. Unlike Meridiani concretions (which are almost pure hematite), Navajo concretions show significant incorporated siliciclastic material, indicative of high pore-fluid velocities. Episodic elevation of the regional water table at Meridiani Planum (McLennan et al., 2005; Andrews-Hanna et al., 2007) would provide stationary pore-waters, consistent with small, incorporated siliciclastic fractions (McLennan et al., 2005; Squyres et al., 2006) and low sphericities (±6%) of Meridiani concretions (Grotzinger et al., 2005). More similar to the Meridiani spherules, semi-soft iron oxide concretions up to a few centimeters in diameter in sandy sediments of acid-saline Lake Brown in Western Australia are in intermediate stages of formation and actively lithify when removed from the lake bed (Bowen et al., 2008). The Yilgarn Craton is Archean continental crust that constitutes the bulk of the Western Australian land mass. It is host to Lake Brown and many other acid-hypersaline, lacustrine environments, which exhibit several depositional and mineralogical similarities to Meridiani Planum including precipitation of evaporites, iron oxides and sulfates during wet episodes and reworking during dry periods (Benison et al., 2007). Furthermore, dating of the surrounding organic-rich sediments of Lake Brown places age limits of between 1410 (±100) and 2913 (±48) years on these concretions (Bowen et al., 2008).

The observed size range of spherules at Meridiani Planum, shown in Table 1, is the result of varying diagenetic conditions during formation and Aeolian reworking. Weathered out loose spherules that litter the soils and gather in topographic depressions can be similar in size to those in neighboring outcrops, which

Table 1
Size and abundance of spherules at Meridiani Planum as measured by McLennan et al. (2005) and Weitz et al. (2006)

Locality	McLennan et al. (2005)			Weitz et al. (2006)	
	Vol.% of host unit occupied	Standard deviation	Spherule-bearing rocks considered	Mean radius (mm)	No of spherules measured
Eagle Crater	1.2	0.4	4	1.98	21
Fram Crater	4.3	0.8	6	–	–
Endurance Crater	4.0	2.0	6	2.24	20
Average for outcrops	3.2	2.0	–	2.11	–
Average for soils	–	–	–	1.44	–

implies their origin. Conversely, some loose spherules can be smaller than spherules embedded in sulfate-rich sediments (Squyres and Athena Science, 2004; McLennan et al., 2005; Weitz et al., 2006). The mean diameter of weathered out spherules is 1.44 mm, while spherules embedded in host rock maintain a larger average diameter of 4.2 mm. Size differences are likely due to differences in source material fluxes during diagenesis or the erosive capabilities of aeolian processes, which leave lags (Chan et al., 2004).

Episodic aqueous recharge is thought to have created the sulfate-rich mineralogy of the Burns formation, which has been interpreted as re-worked evaporite minerals by Squyres et al. (2006). During recharge, iron could have been supplied to form the hematitic spherules in various ways. Fe^{2+} from dissolution of basaltic phases and ferrous sulfates would have been subject to low-temperature oxidation. Ferric sulfates may have occupied 15–40 vol.% of the Burns formation in the form of vugs and crystal moulds (Clark et al., 2005; McLennan et al., 2005). It is possible that some dissolution of iron sulfates to form secondary porosity may have been contemporaneous with the formation of the hematite (McLennan et al., 2005), in which case the iron could have been supplied locally. Once ferric ions appear in solution they are highly susceptible to form Fe-hydroxides, such as ferrihydrite, a reddish-brown insoluble gel (Cornell and Schwertmann, 1996). Once emplaced as a proto-concretion, this precipitate would subsequently dehydrate to goethite and then to hematite over time (Nordstrom and Munoz, 1994; Catling and Moore, 2003; Chan et al., 2007).

Through application of diffusion-based diagenetic models, we here provide insight into the likely formation timescales of the hematitic concretions in the Burns formation and deduce the sources of iron from the modeled supply rates.

2. Diffusion-based diagenetic models

We consider a variety of diffusion-based models that concern only the transport of Fe ions to the growth surface of a concretion. These models were originally developed for growth of calcite concretions (Berner, 1968; Lasaga, 1979; Wilkinson and Dampier, 1990; Wilkinson, 1991; Lasaga, 1998). In our study, the models are applied to a steady-state replenishment of Fe^{2+} or Fe^{3+} to the surface of the concretion. We calculate growth times based on parameters such as concretion size, diffusion coefficients, etc. and their plausible ranges based on

our current knowledge of the Burns formation and the early Martian surface environment.

2.1. Concretion growth mechanisms

A concretion grows when a solute, dissolved in the pore-fluid, precipitates onto its surface (Fig. 1). What initiates precipitation in many concretions is unknown, though usually in terrestrial environments it is an organically derived nucleus or chemical homogeneity. The growth of a concretion is limited by the rate at which the precipitating component is transported into the region of growth. Transport can be accomplished via molecular diffusion or pore-fluid flow. The loss of solute onto the concretion surface results in a zone around the concretion where the solute is of reduced concentration. This concentration is governed by the rates of dissolution at the concretion surface and replenishment of more solute-rich fluid from the surrounding pore-waters. If the concretion's growth rate is limited by the lack of replenishment of the species to the depletion halo then the process is said to be transport controlled. Conversely, if replenishment (by diffusion or pore-fluid motion) is ample, then the system is surface-reaction controlled — limited by the rate at which the molecular species is able to react and attach itself to the concretion surface (Berner, 1968). Assuming no surface-reaction limit, the rate at which the species is transported into the depleted zone determines the rate of concretion growth. A mobile pore-fluid can increase the transport material to the concretions halo and thus increase the rate of growth, so long as growth is not surface-reaction controlled. A stationary pore-fluid results in the flux of material to the growth halo being governed only by molecular diffusion. A system's tendency towards chemical equilibrium drives diffusion while external hydrological processes govern pore-fluid motion through the diagenetic zone. Both molecular diffusion and pore-fluid motion are affected by the physical characteristics of the sedimentary host, e.g. porosity, pre-emplaced salt-fraction volume and grain-size distribution.

The spherical shape and uniform size distribution of the concretions at Meridiani Planum suggest that the diagenetic event that formed them was not driven by energetic, externally impressed lateral flow, so that source materials may have been transported largely by diffusion. In contrast, when lateral flow is important, concretions are found to be elongated (Mozley and Davis, 2005). According to Berner (1968), growth time t, depends on concretion radius r_c, the ionic diffusion coefficient of the source material D_i, the molar volume of the cement v, and the concentration gradient of source material between the surface of the concretion and a large distance ΔC, as follows:

$$t = \frac{r_c^2}{2 v D_i \Delta C} \tag{1}$$

This expression was corrected by Wilkinson and Dampier (1990) and Lasaga (1998) to allow for a non-linear concentration gradient in the depletion halo:

$$t = \frac{r_c^2 F_c}{2 D_i \phi \Delta C v} \tag{2}$$

The correction lies in the term used to describe the flux of material to the surface of the concretion. Porosity of the host rock ϕ, and the volume fraction of host rock that is occupied by concretions F_c, are introduced here. Eqs. (1) and (2) both describe a simple diffusion model, i.e. one in which the host rock serves as a recipient of externally sourced solute and pore-fluids are stationary. Berner (1968) considered the relative motion of the pore-fluid about the concretion and its effects on growth rates, which modifies the growth time to

$$t = \frac{\left(r_c - \frac{D_i}{0.715 u}\right)\left(1 + \frac{r_c u}{D_i}\right)^{0.715} + \left(\frac{D_i}{0.715 u}\right)}{1.715 u v \Delta C} \tag{3}$$

where u is the speed of the mobile pore-fluid.

The movement of pore-fluid increases the flux of source material to the surface of the concretion and (provided that the growth of the concretion is not surface-reaction controlled) growth rates are increased. Wilkinson and Dampier (1990) discuss the ratio of locally provided solute to that which is transported from outside into the depleted zone marked by the dotted line in Fig. 1. It is convenient to define F_d as the volume fraction of the host rock occupied by source material before concretion formation (i.e. iron contained in ferrous and ferric sulfate minerals) and F_p as the volume fraction of precipitate in the concretion after growth has ceased (see erratum by Wilkinson (1991)). For a source to count as external, a major portion of it must have been transported over at least several meters. This is the case for the Navajo sandstone, where the amount of iron present in concretions is greater than that which
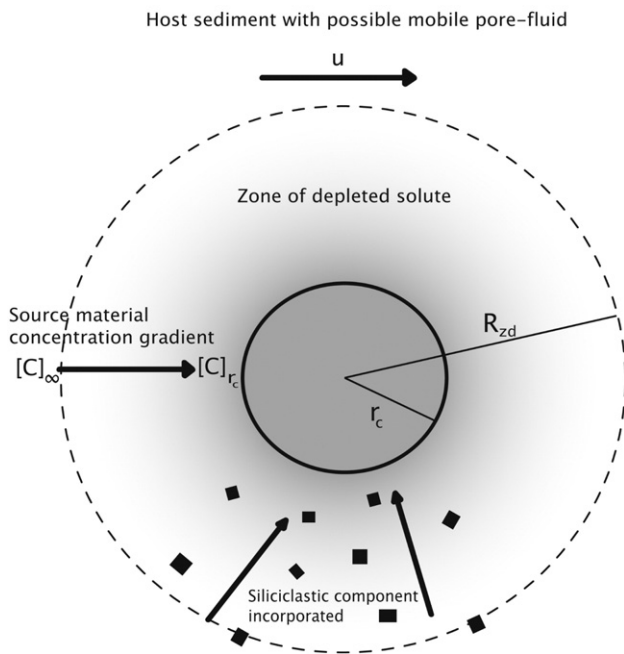

Fig. 1. Schematic for concretion growth. Where: $[C]_\infty - [C]_{r_c} = \Delta C$ is the concentration gradient of the cementing material, r_c is the radius of the growing concretion, R_{zd} is the radius of the depleted zone and u is the velocity of the pore-fluid.

is likely to have been sourced in the immediate vicinity (Chan et al., 2005).

If $F_d/F_p=0$ then a simple growth model is in effect, whereby no material originates from the host rock and all precipitate is externally sourced. If this is not the case, i.e. the host rock plays some role in sourcing the precipitate, then the model is regarded as diagenetic redistribution. Sedimentary rocks at Meridiani Planum in which the concretions are found are ∼ 35–45% sulfate±chloride cements (Clark et al., 2005). The host rock is therefore a likely candidate for supplying the reactants for concretion formation (Chan et al., 2004; McLennan et al., 2005; Tosca et al., 2005). In the concretion formation model of Chan et al. (2004), applied to Utah's Navajo sandstone concretions, thin hematite films that coat individual sand grains represent 0.18–1.25 wt.% of the host rock and provide the source of iron that is leached out to supply concretion growth (Beitler et al., 2003). This magnitude is comparable to values of ∼ 1.0 vol.% (i.e. $F_d=0.01$) suggested for the Burns formation at Meridiani Planum (see Table 1) and indicates the potential importance of considering a growth model that incorporates diagenetic redistribution. Wilkinson and Dampier (1990) accounted for diagenetic redistribution in the simple (Eq. (1)) and mobile pore-fluid (Eq. (3)) models of Berner (1968), respectively as follows:

$$t = \frac{r_c^2\left(1-\left(F_d/F_p\right)^{\frac{1}{3}}\right)}{2vD_i\Delta C} \tag{4}$$

$$t = \frac{\left[\left(r_c-\frac{D_i}{0.715u}\right)\left(1+\frac{r_cu}{D_i}\right)^{0.715}+\left(\frac{D_i}{0.715u}\right)\right]\left[1-\left(\frac{F_d}{F_p}\right)^{\frac{1}{3}}\right]}{1.715uv\Delta C} \tag{5}$$

In a solution of infinite dilution, we would assume a collision-free path for dissolved ions. However, in high ionic strength

brines we note that diffusive processes may be inhibited by ion–ion interactions. For the pore-fluids of sandstone, dissolved iron ions that end up at the concretion surface must navigate a path involving only pore space. The ion diffusion coefficient is given by Iversen and Jørgensen (1993) as

$$D_i = \frac{D_i^0}{1+n(1-\phi)} \tag{6}$$

where $n=2$ for sandy sediments, D_i^0 is the diffusion coefficient for a dilute solution and ϕ is porosity. There are no direct measurements of porosity of the Burns formation, though estimates place it at around 0.2 (see Table 2). There are however, caveats associated with the assumption that the Burns formation is a geometrically idealized sandstone, e.g. an assemblage of close-packed spheres where all pore space is 100% connected. This may not be the case; in a salt-dominated rock, porosity is likely to adopt a microkarstic nature. Through salt cementation, pores may be infilled by clastic assemblages or isolated by the formation of vesicle-like enclosures. This would inhibit brine migration and reduce the overall ionic diffusive equilibration. The quantitative effects of these processes on porosity are not well characterized and we therefore assume a wide range of porosities, with lower and upper limits of 0.05 and 0.30, in order to account for such uncertainties. These figures represent only the pore space available for participation in fluid migration and so essentially the porosity is effective.

We take a value at 0 °C of the ionic diffusion coefficient D_i of the source material because concretion growth is a near-surface process and the freezing point of pure water represents an upper limit for the freezing point of brines. The diffusion coefficient for the ferrous iron ion Fe^{2+}, in infinite dilution at 0 °C is $D_{Fe2+}^0=3.41\times10^{-10}$ m^2 s^{-1}. The Stoke–Einstein relation allows us to calculate $D_{Fe3+,0\,°C}^0$ from

Table 2
Parameter space used in the diffusion-based concretion growth models

Parameter	Meaning	Range/constant	Supporting literature
r_c	Radius of concretion	$0.5<r_c<2.5$ mm	Weitz et al. (2006)
D_{Fe2+}	Molecular diffusion coefficient of Fe^{2+} in pore-fluid.	$1.18<D_{Fe2+}<1.42\,(\times10^{-10})\,m^2\,s^{-1}$	Iversen and Jørgensen (1993)
D_{Fe3+}	Molecular diffusion coefficient of Fe^{3+} in pore-fluid.	$9.55\times10^{-11}<D_{Fe3+}$ $<1.15\times10^{-10}\,m^2\,s^{-1}$	Li and Gregory (1974)
F_c	Volume fraction of the host rock occupied by concretions.	$0.012<0.032<0.043$	McLennan et al. (2005)
F_d	Volume fraction of the host rock occupied by source material (i.e. Fe^{2+} and Fe^{3+}) before concretion formation.	0.01	Clark et al. (2005). Also see Catling and Moore (2003), Chan et al. (2004), Tosca et al., (2005), McLennan et al. (2005). In Navajo Sandstone 0.18–1.25 wt.% exists in hematite films coating individual sand grains before flushing events (Beitler et al., 2003).
F_p	Volume fraction of the concretion occupied by precipitated material.	$0.5<0.7<1.0$	McLennan et al. (2005)
Φ	Porosity of the host rock.	$0.05<0.2<0.3$	Tosca et al. (2005) use maximum fluid-rock ratio of 0.3. Cordova (1978) calculates 0.17 for Navajo Sandstone. Compact terrestrial sandstones may reach 0.05.
v	Molar volume of precipitate, $Fe(OH)_3$.	$v_p=28.12\times10^{-6}\,m^3\,mol^{-1}$	Derived from density and atomic weight.
ΔC	Source material concentration gradient between the surface of the concretion and that of a point a great distance away (i.e. A point outside the depleted zone).	$1<\Delta C<5$ ppm	10^{-4} molar=5.6 mgl^{-1}≈5 ppm Catling and Moore (2003). 3 ppm Tosca et al. (2005)
u	Pore-fluid velocity.	$10^{-3}<10^3$ m/yr No default.	Berner (1968) uses 0.3 to 300 m/yr, which covers the range for terrestrial groundwater.

$D^0_{Fe3+,25 \, ^\circ C}$, via $D^0_{Fe3+,25 \, ^\circ C}/D^0_{Fe3+,0 \, ^\circ C}=2.19\pm0.07$ to give $D^0_{Fe3+,0 \, ^\circ C}=2.77\times10^{-10} \, m^2 \, s^{-1}$ This relationship holds well between 0 °C and 25 °C (Li and Gregory, 1974), but is unconstrained for brines at temperatures below 0 °C. Actual diffusion coefficients, D_{Fe2+} and D_{Fe3+}, can then be calculated from Eq. (6) using appropriate values of porosity.

3. Results

Fig. 2 shows that growth times of between 100 and 2500 yr are obtained for hematitic concretions using stationary pore-fluid models. The most applicable model is likely that of Wilkinson and Dampier (1990) (Fig. 2b), because it accounts for diagenetic redistribution of source material, i.e. resupply of aqueous iron partially from soluble phases that occupied pore space in the host rock prior to diagenesis of the concretions. This produces growth times of between 350 and 1900 yr for an average-sized concretion of 4.2 mm diameter. Prior to the application of these models to hematite concretions on Mars,

only one brief estimate has been placed on Meridiani concretion growth rates, "timescales of significantly less than 10^3 martian years" (McLennan et al., 2005). Applying the parameter domain to the mobile pore-fluid models of Berner (1968) (Eq. (3)) and Wilkinson and Dampier (1990) (Eq. (5)), we calculate significantly smaller growth times (Fig. 3). For an average-sized 4.2 mm diameter concretion and a flow velocity as given in Table 2, the models predict growth times of 1 to 2 weeks.

The large iron fluxes implied by these relatively short growth times would require pore-fluids with high concentrations of Fe^{3+}, since the system would almost certainly be surface-reaction limited by slow oxidation of Fe^{2+} (see Section 4.4). A cryogenic, hypersaline and acidic pore-fluid could carry such high iron concentrations of ferric iron (Marion et al., 2008), though this would probably be subject to lower diffusion coefficients and increased viscosity, which would work to lengthen growth times. Nevertheless, we cannot completely discount the possibility that a mobile pore-fluid was involved because iron-rich cryogenic hypersaline acidic brines may be capable of delivering the high ionic fluxes required for such short growth times. The value of our favoured immobile diffusion-limited models is that they place upper limits on the duration of concretion growth.

For our calculations, we have assumed groundwater flow to be 10^{-3}–$10^3 \, m \, yr^{-1}$ (Table 2), but terrestrial groundwater systems in sandstones can possess much higher flow velocities of up to ~10 km yr^{-1} due to low porosity and higher hydraulic head. To test the feasibility of this on Mars, we could set pore-fluid velocity, $u=10 \, km \, yr^{-1}$ and constrain growth time to $t=100$–2500 yr in the mobile pore-fluid models (Eqs. (3) and (5)) to solve for concretion radius. For a dilute fluid ($[Fe^{2+}]=10^{-4}$ M) at 0 °C, this produces concretions several meters in diameter, which are not observed at Meridiani Planum. There is a range of intermediate possibilities in this case. If the fluid were hypersaline, cryogenic and acidic, higher iron loading could encourage growth of large concretions over these timescales, while the higher viscosity and lower diffusion rates incurred would work to the contrary. Nevertheless, high concretion sphericities noted by McLennan et al. (2005) support the argument that fluids were relatively stationary at Meridiani Planum during concretion growth since adhesive flux of cementing materials would be spherically symmetrical in an isotropic pore-fluid. Diffusive transport of source material would be less energetic and driven by concentration gradients. The resulting ionic flux would be much less likely to pull along siliciclastics. The flushing events described for concretions in Navajo sandstone by Chan et al. (2004) imply relatively high pore-fluid flux compared to the more stagnant conditions likely experienced at Meridiani Planum through upwelling of groundwaters suggested by Andrews-Hanna et al. (2007). Regional elevation of the water table would allow diagenetic recharge without significant lateral movement of pore-waters within the Burns Formation.
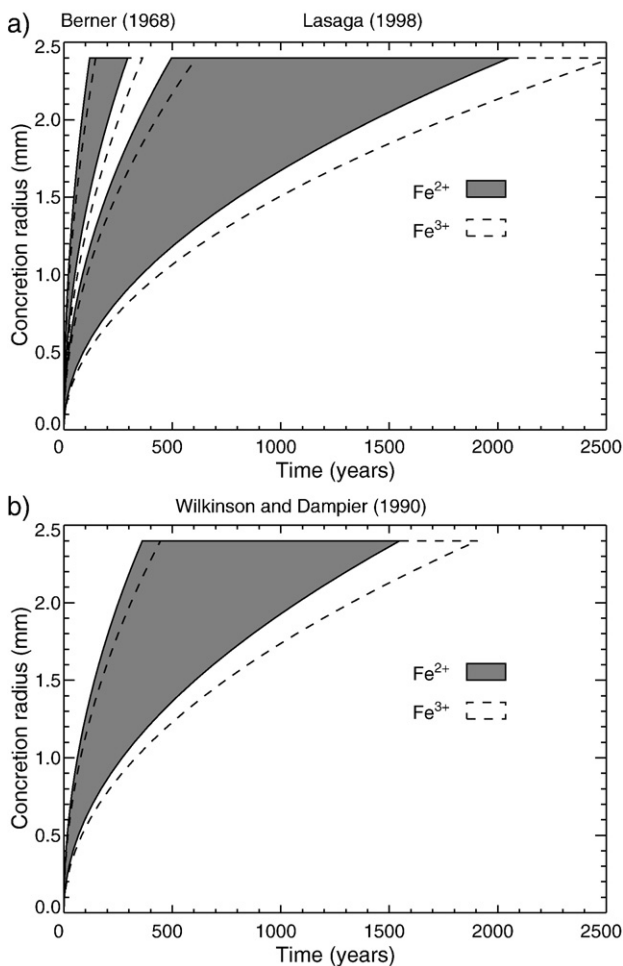

Fig. 2. The range of concretion growth times calculated using upper and lower limits of parameters estimated for conditions at Meridiani Planum (see Table 2) applied to stationary pore-fluid models. a) The simple models of Berner (1968) (Eq.(1)) and Lasaga (1979, 1998) (Eq. (2)), the latter of which corrects for a non-linear concentration gradient in the depleted zone. b) The diagenetic redistribution model of Wilkinson and Dampier (1990) (Eq. (4)).

3.1. Limitations of diffusion-based models

As a caveat, we note that our results, founded on diffusion-based models, consider the growth time only as the
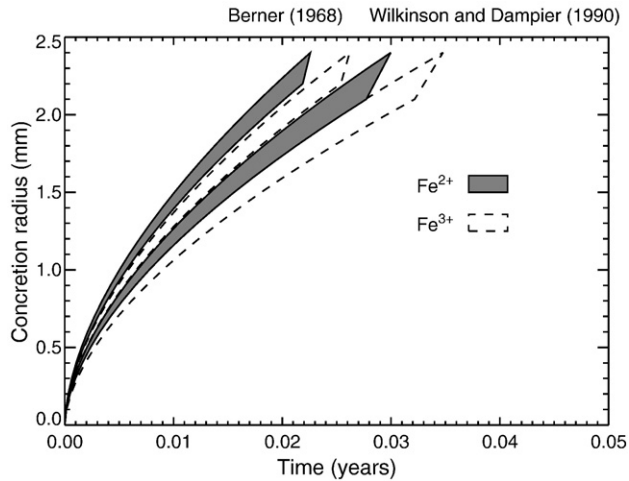
Fig. 3. The range of concretion growth times calculated using upper and lower limits of parameters estimated for conditions at Meridiani Planum (see Table 2) applied to the mobile pore-fluid models of Wilkinson and Dampier (1990) (Eq. (5)) and Berner (1968) (Eq. (3)). The pore-fluid velocity is varied from 1 mm to 1 km yr^{-1}. These concretion growth times are of the order of 1 to 2 weeks and are thus unrealistically short, as reaction kinetics at the surface of the concretion are not likely to proceed at a sufficient rate to ultimately provide all the hematite we observe.

time taken for sufficient source material to migrate to a growing concretion's surface. They do not consider inhibition to precipitation of the source iron as ferric hydroxides by reaction rate limitations such as oxidation of dissolved Fe^{2+} and the rate of dissolution of pre-emplaced ferric and ferrous sulfates. These could increase the timescale, although precipitation of iron oxides is so rapid that kinetic data remain unmeasured. We may not necessarily discount the possibility of pore-fluid mobility. It is unlikely to be large only for dilute fluids at 0 °C. If cryogenic, hypersaline, acidic fluids were dominant then a degree of pore-fluid mobility is plausible, since the models are unable to account for the increased viscosity and higher ionic strength kinetics at low temperatures.

As previously stated (see Section 2.1) precipitation of salts may enclose and isolate porosity, reducing the pore space available for interaction with diagenetic fluids. This sealing-off process cannot be accounted for in the models except by utilising a large range of values for porosity. Once formed, ferric hydroxides would take time to undergo paragenesis and dehydrate to goethite and then hematite. Fischer and Schwertmann (1975) observed complete transformation of ferrihydrite to hematite at 70 °C over periods of hundreds of hours to several weeks. At 20 °C, Schwertmann and Murad (1983) show a half-conversion time of 112 days at pH 7. It is possible that temperatures were a great deal lower at Meridiani Planum and so timescales were longer, unless mildly hydrothermal pore-fluids helped to sustain warm near-surface temperatures.

Finally, we note that all natural terrestrial environments have microbiology and so cannot be perfect analogues due to the inevitable biomediation that occurs during concretion growth on Earth.

4. Discussion

Given our estimates of the growth time of concretions and the observed amount of hematite in the stratigraphy, we can examine the rates of iron delivery required to place some constraints on the likely source of the iron.

4.1. Total Fe^{3+} required

The Fe^{3+} contained in the concretions in 1 m^3 of the Burns formation ranges from (2 mol Fe^{3+} per mol Fe_2O_3)×(0.012×0.5)/ (30.48×10^{-6} m^3 mol^{-1} Fe_2O_3)=394 mol Fe^{3+} m^{-3} for a 50 vol.% Fe_2O_3 concretion embedded in the Eagle Crater outcrop (1.2 vol.% host rock occupancy of spherules) to 2×(0.043×1.0)/30.48× 10^{-6}=2822 mol Fe^{3+} m^{-3} for a 100 vol.% Fe_2O_3 concretion embedded in the Fram Crater outcrop (4.3 vol.% host rock occupancy of spherules). The required ferric iron could be produced via oxidation of dissolved Fe^{2+} (from dissolution of ferrous sulfates or basaltic phases) or supplied via dissolution of ferric sulfates. We now consider both supply mechanisms.

4.2. Supply of Fe^{2+} from dissolution of basaltic phases

Dissolution of Fe^{2+} from basaltic phases on Mars is comparatively slow and probably provided a negligible contribution to the concretion-forming iron, as we now demonstrate. The rate of dissolution of Fe^{2+} from basaltic phases depends on pH, ionic strength and temperature. The dissolution rate of Fa_{33} (33% fayalite, $Fe^{2+}_2SiO_4$, and 67% forsterite, $Mg^{2+}_2SiO_4$), which is compositionally similar to olivine in Shergottite, Nakhlite and Chassignite (SNC) meteorites, is estimated to be 0.5 ppm Fe^{2+} m^{-2} yr^{-1} (9.46×10^{-6} mol m^{-2} yr^{-1}) at 1 °C and pH 4.5 (Burns, 1993).

However, in order to know the possible contribution of Fe^{2+} from this phase to concretion-forming iron, we must know the olivine surface area in contact with dissolving fluids per cubic meter of the basaltic host. Geometrically calculated internal surface areas of porous materials may be calculated based on idealized geometries. A form of the Kozeny–Carman equation (Carman, 1956; Paterson, 1983) relates permeability, k to porosity, ϕ by $k=\phi^2/\Lambda Fs^2$ where Λ is a constant equal to 2 if the connections between pores are cylindrical, s is the internal surface area and F is the formation factor of the rock. F is determined by Archie's law, $F=\phi^{-m}$, where $m=2$ for sub-spherical vesicles/pore spaces (Saar and Manga, 1999) or 1.3 for sandy soils (Sen et al., 1981). Substituting and rearranging for s we find that $s=(\phi^{(2+m)}/2k)^{1/2}$. We therefore apply weathering rates presented by (Burns, 1993) to calculated plausible maximum and minimum surface areas in contact with weathering fluids at Meridiani Planum.

Firstly, we consider a rock similar to the basaltic shergottites, which would show minor olivine (Bridges and Warren, 2006) and a permeability of $k≈10^{-17}$ m^2 (Saar and Manga, 1999). Assuming 1 wt.% olivine and a porosity of 0.02 (Beech and Coulson, 2005) we calculate an Fe^{2+} production flux of between 0.8 and 25.4 mol Fe^{2+} m^{-3} in 100 and 3000 yr respectively.

Secondly, for an unconsolidated soil similar to that of a basaltic soil found at Meridiani Planum with porosity 0.4 (Clifford, 1993), permeability $k \approx 10^{-11}$ and olivine content 40 wt.% (Klingelhöfer et al., 2004; Squyres and Athena Science, 2004) we calculate an Fe^{2+} production flux of between 296 and 8882 mol Fe^{2+} m^{-3} in 100 and 3000 yr respectively.

The dissolution rate and therefore total Fe^{2+} supply from olivine is highly pH dependant, e.g. it may be 350 times faster at pH 2 (Burns, 1993). Though this may increase the Fe^{2+} supply flux in more acid solutions, a number of factors would work to lower it. 1) The reactive surface area changes as olivine is dissolved so any calculation involving application of weathering rates to a fixed surface area may not be accurate. 2) Pore space in rocks is unlikely to be 100% interconnected and isolated pores would not contribute to reactive surface area. 3) Non-ideal morphology of connected pore space may be inhibitive to flow or ionic diffusion. This cannot easily be accounted for mathematically. 4) If ferrihydrite precipitates from reaction with dissolved ferrous iron, oxygen and water, the iron-supplying crystals may develop ferrihydrite coatings, which armor the crystal boundaries and thus inhibit further dissolution of Fe^{2+} (Burns, 1993). 5) If dissolution of a mineral surface progresses preferentially in some areas, etch pits are formed. These increase the available surface area for further dissolution, but concurrently reduce the ability of a fluid to flow over the new surface since an isolated well is formed. 6) Although olivine-rich, gardened surface regolith may potentially supply a large fraction of the concretion-forming iron, it would be the unit saturated for the least amount of time during recharge, due to its stratigraphic position and the upwelling nature of diagenetic fluids (Andrews-Hanna et al., 2007). 7) Finally, the soil at Meridiani contains olivine and so it was clearly not completely weathered.

4.3. Supply of Fe^{2+} from dissolution of a ferrous sulfate

Melanterite ($Fe^{2+}SO_4 \cdot 7H_2O$) is an abundant product in evaporative modeling of fluids derived from weathered basaltic material likely to precede the evaporate mineralogy at Meridiani Planum. Its formation is favoured at high Fe^{2+}/Fe_T ratios, while jarosite ($KFe^{3+}3(OH)_6(SO_4)_2$) is the dominant evaporite product from fluids of high ferric content (Tosca et al., 2005). Melanterite is a candidate mineral for occupying up to 8% of the host rock porosity, which ranges from 15–40% at observed Meridiani outcrops (McLennan et al., 2005). This gives a melanterite volume occupancy in the range 1.2–3.2%, potentially supplying 82–218 mol Fe^{2+} m^{-3}. This is below the estimated 394–2822 mol Fe^{3+} m^{-3} needed, but could be a significant portion of the concretion-forming iron, at the lower requirement limit.

4.4. Oxidation rates of aqueous Fe^{2+}

Once Fe^{2+} is in solution, ferrous ions would need to be subsequently oxidized to Fe^{3+} in order to precipitate. Therefore, for any iron supplied to the concretion surface as Fe^{2+}, as discussed above, the rate of precipitation must be controlled by the oxidation rate of Fe^{2+} in a pore-fluid interacting with the early Martian atmosphere.

The oxidation rate of Fe^{2+}(aq) can be described as a function of its concentration $[Fe^{2+}]$, pH, partial pressure of oxygen, (pO_2), temperature T (K), and ionic strength I, of the solution (Millero and Izaguirre, 1989), as follows:

$$\frac{d[Fe^{2+}]}{dt} = -k_B [Fe^{2+}](pO_2)[OH^-]^2 \tag{7}$$

where: $[OH^-]^2 = \frac{K_w^2}{10^{2pH}}$ and:

$$\log k_B = 21.56 - 1545/T + A\sqrt{I} + B\sqrt{I}/T + CI$$

Here, K_w is the dissociation constant for water. Taking logarithms and substituting for $[OH^-]^2$, we may describe the rate of creation of Fe^{3+} ions by:

$$\frac{d}{dt}\log[Fe^{3+}] = \log k_B + \log[Fe^{2+}] + \log(pO_2) + 2(pK_w - pH) \tag{8}$$

During the Noachian, when volcanism was common, any atmospheric oxygen would be rapidly removed by oxidation of volcanic products (Catling and Moore, 2003; Zahnle and Haberle, 2007). Consequently, in the Noachian, when concretion growth took place, atmospheric oxygen content and thus iron oxidation rates were likely to be lower than today. The estimated partial pressure of oxygen, pO_2, may have been as low as 10^{-12} bar, which would significantly limit the oxidation of Fe^{2+} in near-surface brines. Because of the unknown oxidation state of the early Martian atmosphere, we assume in our model the present-day value of 10^{-5} bar as a maximum bound. We set Fe^{2+} concentration to 10^{-4} M, equivalent to 5.6 mg l^{-1} Fe^{2+}, which is reasonable for an iron-rich fluid (Catling and Moore, 2003). Temperature is assumed to be 0 °C and the log of the dissociation constant of water pK_w ($-\log_{10}(K_w)$) is set to 13.63, corresponding to a brine at 0 °C with ionic strength 1.

Burns (1993) applied the relationship described in Eq. (8) to the oxidation of Fe^{2+} produced from weathering of ferromagnesian minerals and predicted that ferrolysis of Fe^{2+} to form insoluble Fe^{2+} hydroxides would occur rapidly when near-neutral pH groundwater becomes saturated with atmospheric oxygen. Thus if we assume that ferric ions readily precipitate as $Fe(OH)_3$ or complexes that convert to $Fe(OH)_3$ (Nordstrom and Munoz, 1994) then we may assume that the rate of precipitation of ferrihydrite is equal to the oxidation rate of Fe^{2+}.

We plot the amount of moles of Fe^{3+} created per cubic meter of fluid in 500 and 1000 yr according to Eq. (8) (Fig. 4). Dotted lines represent the amount required to create the hematite contained in concretions at Fram ($F_c = 0.043$) and Eagle ($F_c = 0.012$) craters. If present-day atmospheric oxygen levels prevailed during concretion diagenesis, fluids would be required to possess a pH of between 6.55 and 7.10. Setting $\log pO_2 = -12$ in the calculations of Fig. 4 yields drastically lower amounts of created Fe^{3+}, just $\sim 10^{-3.30}$–$10^{-4.75}$ ($\approx 5.01 \times 10^{-4}$–$1.78 \times 10^{-5}$) moles Fe^{3+} m^{-3} in the same pH range. The calculations require standing, near-neutral, surface brines and present-day atmospheric oxygen content to produce sufficient Fe^{3+} to form the observed concretions. Given that atmospheric oxygen pressure was probably much
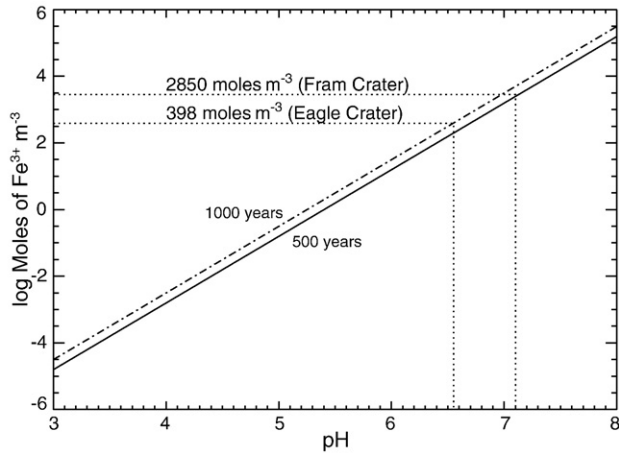
Fig. 4. Log moles of Fe^{3+} m^{-3} of the Burns formation with an assumed porosity of 0.2 produced by oxidation of aqueous Fe^{2+} in a 10^{-4} molal (5.6 mg L^{-1}) solution at 0 °C and $pO_2=10^{-5}$ bar (present-day value) over 500 and 1000 yr according to the relationship of Burns (1993). Oxidation rates are strongly dependant on pH. Dotted lines represent amounts of Fe^{3+} required to produce the Fe^{3+} contained in hematite observed in concretions at Fram and Eagle craters. If all the Fe^{3+} in concretions were to be sourced by oxidation of Fe^{2+}, given our growth times, diagenetic pore-fluids would have to maintain a pH of 6.55–7.10.

lower during the Noachian, Fig. 4 places an upper limit on the amount of ferric iron available for concretion growth that may be created from oxidation of Fe^{2+}. It is possible, but unlikely, that most concretion-forming ferric iron was supplied from oxidation Fe^{2+}. A significant fraction of the Fe^{3+} was probably supplied from dissolution of ferric sulfates, which we discuss in Sections 4.5 and 4.6.

With regard to alternate methods of Fe^{2+} oxidation, photo-oxidation of ferrous iron complexes by the photo-stimulated release of hydrogen gas would not be a viable method because the concretions formed below the surface, away from sunlight.

4.5. Supply of Fe^{3+} from dissolution of jarosite

The dissolution rate of a given mineral depends on the temperature, pH, the activation energy of the dissolution reaction, the activities of other species in solution, (which may provide possible catalytic or inhibitory effects (Lasaga, 1998)), and the degree of saturation Ω, which is equal to the ion activity product (IAP) of the dissolved species divided by the solubility product of the original compound i.e. $\Omega=\text{IAP}/K_{sp}$. If dissolution is to occur, Ω must be less than unity.

Baron and Palmer (1996) conducted solubility studies of jarosite through dissolution experiments at 4 to 35 °C and at pH 1.5–3. Equilibrium was attained after 80–125 days and the dissolution reaction was described by a first-order model. Hydronium jarosite (H$_3$O·Fe^{3+}3(SO$_4$)$_2$(OH)$_6$), with a log K of −90.1 for the solid-solution equilibrium shown in Table 3, is significantly more soluble than pure K-jarosite (K.Fe^{3+}3(SO$_4$)$_2$(OH)$_6$), with a log K for the solid-solution equilibrium shown in Table 3 of −95.8 under standard conditions (see also Chapman et al. (1983) and Kashkay et al. (1975)). Just one dissolution rate constant of potassium ions was obtained for K-jarosite from experiments at pH 2 and at 25 °C: $k=7.9\times10^{-7}$ mol K$^+$ l^{-1} s^{-1}. If congruent dissolution of K-jarosite occurred then Fe^{3+} would dissolve at a rate similar to that of potassium ions and the dissolution rate would be 24.9 mol Fe^{3+} l^{-1} yr^{-1} (Baron and Palmer, 1996). The jarosite component of the Burns formation is estimated to be 10% (McLennan et al., 2005). If there was a similar amount prior to the concretion-forming diagenetic event that has been lost, and we assume that porosity $\phi=0.20$, then the amount of Fe^{3+} produced is equal to $0.10k\phi\rho_w$, where ρ_w is the density of water. This yields 498 mol Fe^{3+} m^{-3} yr^{-1}, suggesting that dissolution of jarosite could have been a significant contributor of ferric iron. If a portion of the jarosite was H$_3$O-jarosite, it is likely that dissolution rates would be increased. Jarosite may well be a significant contributor

Table 3

Candidate soluble ferric sulfates that could have been emplaced in secondary porosity in the Burns formation and contributed to the supply of concretion-forming Fe^{3+}

Mineral	Formula	Solid-solution equilibrium	Solid's free energy of formation ΔG_f^0 (kJ mol^{-1})	$\log_{10}K$
Coquimbite[1]	Fe$_2^{3+}$(SO$_4$)$_3$·9H$_2$O	Fe$_2^{3+}$(SO$_4$)$_3$·9H$_2$O (s)=2Fe^{3+}(aq)+3SO$_4^{2-}$(aq)+9H$_2$O (l)	−4250.6[a]	26.0
Kornelite[1,*]	Fe$_2^{3+}$(SO$_4$)$_3$·7H$_2$O	Fe$_2^{3+}$(SO$_4$)$_3$·7H$_2$O (s)=2Fe^{3+}(aq)+3SO$_4^{2-}$(aq)+7H$_2$O (l)	−3793.7[a]	22.9
Rhomboclase[1]	Fe$_2^{3+}$(SO$_4$)$_3$·H$_2$SO$_4$·8H$_2$O	Fe$_2^{3+}$(SO$_4$)$_3$·H$_2$SO$_4$ ·8H$_2$O (s)=2Fe^{3+}(aq)+4SO$_4^{2-}$(aq)+2H$^+$(aq)+8H$_2$O (l)	−2688[e]	−41.2
Bilinite[1,2]	Fe^{2+}Fe$_2^{3+}$(SO$_4$)$_4$·22H$_2$O	Fe$_3$(SO$_4$)$_4$·22H$_2$O (s)=Fe^{2+}(aq)+2Fe^{3+}(aq)+4SO$_4^{2-}$(aq)+H$_2$O (l)	−8410[a]	−16.4
Yavapaiite[2,*]	KFe^{3+}(SO$_4$)$_2$	KFe^{3+}(SO$_4$)$_2$ (s)=K$^+$(aq)+Fe^{3+}(aq)+2SO$_4^{2-}$(aq)	−1818.8[b]	−5.6
Copiapite[1,2]	Fe^{2+}Fe$_4^{3+}$(SO$_4$)$_6$(OH)$_2$·20H$_2$O	Fe$_5$ (SO$_4$)$_6$(OH)$_6$·20H$_2$O (s)=Fe^{2+}(aq)+4Fe^{3+}(aq)+6SO$_4^{2-}$(aq)+2OH$^-$(aq)+ 20H$_2$O (l)	−9971[a]	−51.5
Fibroferrite[2]	Fe^{3+}(SO$_4$)(OH)·5H$_2$O	–	–	–
K-jarosite	KFe$_3^{3+}$(SO$_4$)$_2$(OH)$_6$	KFe$_3^{3+}$(SO$_4$)$_2$(OH)$_6$ (s)=K$^+$(aq)+3Fe^{3+}(aq)+2SO$_4^{2-}$(aq)+6OH$^-$ (l)	−3309.8[c]	−95.8
Hydronium jarosite	(H$_3$O)$^+$Fe$_3^{3+}$(SO$_4$)$_2$(OH)$_6$	(H$_3$O)Fe$_3^{3+}$ (SO$_4$)$_2$(OH)$_6$ (s)=H$_3$O$^+$(l)+3Fe^{3+}(aq)+2SO$_4^{2-}$(aq)+6OH$^-$(l)	−3232.3[d]	−90.1
Melanterite (ferrous)	Fe^{2+}SO$_4$·7H$_2$O	Fe^{2+}SO$_4$·7H$_2$O (s)=Fe^{2+}(aq)+SO$_4^{2-}$(aq)+7H$_2$O (l)	−2507.8[a]	−2.3

*Monoclinic and therefore a candidate for occupying crystal-moldic pores, although it is most likely that Melanterite, a ferrous sulfate, occupied these.
[1]Predicted to form from evaporite recharge modelling by Tosca et al. (2005).
[2]Ferric sulfates thought to exist in Paso Robles soils at Gusev crater from MER-A (Spirit) APXS data (Lane et al., 2007). Refs.: a. Hemingway et al. (2002) b. Forray et al. (2005) c. Baron and Palmer (1996) d. Drouet and Navrotsky (2003) e. Majzlan et al. (2006).
The logarithm to the base 10 of the equilibrium constant K, for solid-solution reactions is calculated according to log $K=-\Delta G_R^0/(2.303RT/1000)$, where ΔG_R^0 is the Gibbs free energy for the reaction in kJ mol^{-1} at standard conditions (298.15 K and 1 bar), universal gas constant $R=8.3144$ J K^{-1} mol^{-1}, and T is temperature in Kelvin. For these calculations, we assumed the following values for the Gibbs free energy of formation in kJ mol^{-1}: ΔG_f(OH$^-$(aq))=−157.3, ΔG_f(H$_2$O(l))=−237.14, ΔG_f(SO$_4^{2-}$(aq))=−744.0, ΔG_f (Fe^{2+}(aq))=−90.53, ΔG_f (Fe^{3+}(aq))=−16.28, ΔG_f (K$^+$(aq))=−282.5. Values for aqueous iron species are taken from Parker and Khodakovskii (1995), whereas other thermodynamic data are from Cox et al. (1989).

to the ferric iron in solution, especially so if upwelling groundwaters had a temperature greater than 0 °C and were acidic (with pH lower than ~3–4).

4.6. Supply of Fe^{3+} from dissolution of other candidate phases

Modelling by Tosca et al. (2005) (using a porosity of 0.30) suggests that evaporative products after diagenetic recharge of Burns formation-like mineralogy include melanterite, bilinite ($Fe^{2+}Fe_2^{3+}(SO_4)\cdot22H_2O$), copiapite ($Fe^{2+}Fe_4^{3+}(SO_4)_6(OH)_2 20H_2O$), goethite (FeOOH) and jarosite. Solubility data for these minerals are listed in Table 3). Coquimbite ($Fe_2^{3+}(SO_4)_3\cdot9H_2O$) and kornelite ($Fe_2^{3+}(SO_4)_3\cdot7H_2O$), which were detected at the Paso Robles soils by the Spirit rover at Gusev crater (Lane et al., 2007), are very soluble (with solubility products given by log K values of 26 and 22.9 respectively), and thus have the highest Fe-supply potential. However, coquimbite and kornelite are not predicted to form as evaporitic products at Meridiani Planum from diagenetic recharge. The jarosite proportion increases significantly with reduction in the Fe^{2+}/Fe_T ratio, while accordingly, melanterite is produced in highest abundance (33.67 mol%) at $Fe^{2+}/Fe_T = 0.90$. We would expect most ferric sulfates to form in parallel with higher jarosite abundance, where the Fe^{2+}/Fe_T is lowest. Less soluble ferric sulfate phases such as bilinite and copiapite may be able to supply a small amount of Fe^{3+} to solution but they are not predicted to form in significant abundance. Phases possessing both di and tri-valent iron have much less solubility (Table 3) and so probably do not contribute significantly to supply of ferric iron. Moreover, according to evaporite modeling (Tosca et al., 2005) very soluble ferric sulfates such as coquimbite and kornelite are produced in low abundance after diagenetic recharge, allowing little ferric iron to be supplied from these phases for formation of ferric hydroxides.

Secondary moldic and vug porosity could have harbored a number of ferric sulfate phases (Table 3), though there is question as to whether these phases were dissolved before or after concretion growth (McLennan et al., 2005). If concretion growth was a secondary porosity-forming event then dissolution of ferric sulfates and concretion growth were possibly contemporaneous, allowing for a portion of the iron in concretions to be sourced from theses phases. But textural evidence suggests that formation of the secondary moldic porosity may post-date concretion growth (McLennan et al., 2005). If concretions formed before secondary porosity then our calculations still allow for sufficient supply of iron from jarosite and ferrous phases in the matrix to grow the concretions.

Mg-sulfates such as epsomite ($MgSO_4\cdot7H_2O$) are evaporite minerals predicted to crystallize at low temperatures from brines (Marion et al., 2003). Another hydrated magnesium sulfate, $MgSO_4\cdot11H_2O$, forms euhedral crystals and may have occupied crystal-moldic porosity. Above 2 °C this phase melts and yields a mixture of 70% epsomite ($MgSO_4\cdot7H_2O$) and 30% H_2O by volume (Peterson and Wang, 2006). Occupation of crystal moulds by Mg-sulfates, instead of Fe-sulfates, would lower the amount of iron available to pore-fluids and thus require that sufficient iron was supplied from

ferric and ferrous sulfates which occupied non-euhedral porosity.

5. Conclusions

Results in Fig. 2 show that modeling the growth of concretions via diffusion-controlled processes yields growth times in the range ~l00–2500 yr. Our preferred model, which incorporates diagenetic redistribution, gives a range of 350–1900 yr (Fig. 2b). Mobile pore-fluid models of Berner (l968) and Wilkinson and Dampier (1990) produce short growth times that are unrealistic when considering the feasibility of iron-supply rates (Fig. 3). Thus the water conditions were likely relatively isotropic and stagnant, which is consistent with regional elevation of the water table, perhaps caused by surface loading of aquifers by Tharsis activity (Andrews-Hanna et al., 2007). The sphericity of the spherules also indicates relatively low flow conditions. The calculated growth timescales are in excellent agreement with radiocarbon dates that constrain a terrestrial analogue of iron oxide concretions in Lake Brown in Western Australia. Radiocarbon dates of organic-rich lake bed sediments above and below concretion-bearing sandy sediments constrain Lake Brown concretion growth times to less than ~3000 yr (Bowen et al., 2008). The ephemeral nature of Lake Brown in Western Australia in addition to its mineralogical and depositional similarities, such as periodic aeolian reworking, hematite cement concretion diameters of 2–40 mm, precipitation of evaporites, iron oxides and sulfates (notably jarosite), provides a good terrestrial analogue to Meridiani.

The precipitation rate of ferric hydroxides is likely to be rapid, and probably not a limiting step in the growth process. A simple diagenetic redistribution model is most applicable because much of the initial source iron is likely to have been pre-emplaced in the form of ferric and ferrous sulfates, which occupied the host rock prior to diagenesis. We estimate that ~394–2822 mol Fe^{3+} m^{-3} are required for concretion formation. Dissolution of basaltic phases was likely a very minor source of Fe^{2+} during concretion diagenesis because, despite supply fluxes from dissolution of olivine in 100 and 3000 yr being calculated as large at pH 4.5, our calculations are subject to multiple inhibiting factors (see Section 4.2), which would probably make the contribution from basaltic phases negligible. Melanterite could have potentially supplied 82–218 mol Fe^{2+} m^{-3} to solution based on the limits of volume occupancy of euhedral secondary porosity at Meridiani outcrops (McLennan et al., 2005). Fe^{2+} supplied to solution from dissolution of both basaltic phases and melanterite therefore potentially supply ~112–248 mol Fe^{2+} m^{-3}, but supply of iron in divalent form is subject to constraints by slow oxidation rates of aqueous Fe^{2+} on early Mars.

In contrast to ferrous iron, mass flux balance suggests that the concretions could have formed from supply of Fe^{3+}(aq) sourced from sediments local to the concretions. The ferric iron would rapidly precipitate out as ferric hydroxide precursors to hematite. Supply of this Fe^{3+} could have occurred predominantly through dissolution of jarosite if conditions were sufficiently acidic and warm. If secondary vug and moldic porosity formation was

contemporaneous with concretion growth, ferric sulfates could have provided minor amounts of Fe^{3+}, though soluble ferric sulfate minerals are not predicted to form in the precursor evaporitic mineralogy (Tosca et al., 2005). Phases that are predicted to crystallize in any noticeable fraction, i.e. bilinite and copiapite, are less soluble, but may have provided some Fe^{3+} in a steady-state system. If formation of secondary vug and moldic porosity post-dates concretion growth (McLennan et al., 2005) then jarosite and ferrous phases were probably significant iron contributors.

Occupation of crystal molds by Mg-sulfates (Chan et al., 2005; McLennan et al., 2005; Peterson and Wang, 2006) would also lower the amount of available iron in the immediate vicinity and require that it be supplied by dissolution of Fe^{2+}- and Fe^{3+}-bearing phases upon ascent of elevated groundwater. In a broader context, our inference that iron-bearing sulfates likely supplied the iron to hematite concretions would explain the spatial association of grey crystalline hematite with sulfates that are observed from orbital spectra at Meridiani Planum, Valles Marineris and in chaotic terrain (Aram, Aureum and Iani Chaos) (Christensen et al., 2001; Bibring et al., 2007; Glotch and Rogers, 2007).

Acknowledgements

References

Andrews-Hanna, J.C., et al., 2007. Meridiani Planum and the global hydrology of Mars. Nature 446, 163–166.

Baron, D., Palmer, C.D., 1996. Solubility of jarosite at 4–35 degrees C. Geochim. Cosmochim. Acta 60, 185–195.

Beech, M., Coulson, I.M., The porosity of Martian meteorite Dar al Gani 476. The 5th Canadian Space Workshop. Canadian Space Agency, Chapman Space Center, Longueuil, Quebec, 2005.

Beitler, B., et al., 2003. Bleaching of Jurassic Navajo Sandstone on Colorado Plateau Laramide highs: evidence of exhumed hydrocarbon supergiants? Geology 31, 1041–1044.

Bowen, B.B., et al., 2008. Active hematite concretion formation in modern acid saline lake sediments, Lake Brown, Western Australia. Earth Planet. Sci. Lett.

Benison, K.C., et al., 2007. Sedimentology of acid saline lakes in Southern Western Australia: newly described processes and products of an extreme environment. J. Sediment. Res. 77, 366–388.

Berner, R.A., 1968. Rate of concretion growth. Geochim. Cosmochim. Acta 32, 477–483.

Bibring, J.P., et al., 2007. Coupled ferric oxides and sulfates on the Martian surface. Science 317, 1206–1210.

Bridges, J.C., Warren, P.H., 2006. The SNC meteorites: basaltic igneous processes on Mars. J. Geol. Soc. (Lond.) 163, 229–251.

Burns, R.G., 1993. Rates and mechanisms of chemical-weathering of ferromagnesian silicate minerals on Mars. Geochim. Cosmochim. Acta 57, 4555–4574.

Carman, P.C., 1956. Flow of Gases Through Porous Media. Academic, San Diego.

Catling, D.C., Moore, J.M., 2003. The nature of coarse-grained crystalline hematite and its implications for the early environment of Mars. Icarus 165, 277–300.

Chan, M.A., et al., 2004. A possible terrestrial analogue for haematite concretions on Mars. Nature. 429, 731–734.

Chan, M.A. et al., 2005. Red rock and read planet diagenesis: Comparisons on Earth and Mars concretions. GSA Today 15, 4–10.

Chan, M.A., et al., 2007. Models of iron oxide concretion formation: field, numerical, and laboratory comparisons. Geofluids 7, 356–368.

Chapman, B.M., et al., 1983. Processes controlling metal-ion attenuation in acid-mine drainage streams. Geochim. Cosmochim. Acta 47, 1957–1973.

Christensen, P.R., et al., 2001. Global mapping of Martian hematite mineral deposits: remnants of water-driven processes on early Mars. J. Geophys. Res.-Planets 106, 23873–23885.

Clark, B.C., et al., 2005. Chemistry and mineralogy of outcrops at Meridiani Planum. Earth Planet. Sci. Lett. 240, 73–94.

Clifford, S.M., 1993. A model for the hydrologic and climatic behavior of water on Mars. J. Geophys. Res. 98, 10973–11016.

Cordova, R.M., 1978. Ground-water conditions in the Navajo Sandstone in the central Virgin River basin, Utah. Utah Dep. Nat. Resour. Tech. Publ. 61, 66.

Cornell, R.M., Schwertmann, U., 1996. The Iron Oxides. VCH, New York.

Cox, J.D., et al., 1989. CODATA Key Values for Thermodynamics. Hemisphere Publishing Corp., New York.

Drouet, C., Navrotsky, A., 2003. Synthesis, characterization, and thermochemistry of K–Na–H_3O jarosites. Geochim. Cosmochim. Acta 67, 2063–2076.

Edgett, K.S., 2005. The sedimentary rocks of Sinus Meridiani: five key observations from data acquired by the Mars Global Surveyor and Mars Odyssey orbiters Mars. Int. J. Mars Sci. Explor. 1, 5–58.

Fischer, W.R., Schwertmann, U., 1975. Formation of hematite from amorphous iron(III)hydroxide. Clays Clay Miner. 23, 33–37.

Forray, F.L., et al., 2005. Thermochemistry of yavapaiite KFe(SO4)(2): formation and decomposition. Geochim. Cosmochim. Acta 69, 2133–2140.

Gendrin, A., et al., 2005. Sulfates in martian layered terrains: the OMEGA/Mars Express view. Science 307, 1587–1591.

Glotch, T.D., Christensen, P.R., 2005. Geologic and mineralogic mapping of Aram Chaos: evidence for a water-rich history. J. Geophys. Res.-Planets 110, 1–21.

Glotch, T.D., Rogers, A.D., 2007. Evidence for aqueous deposition of hematite- and sulfate-rich light-toned layered deposits in Aureum and Iani Chaos, Mars. J. Geophys. Res.-Planets 112, 1–11.

Grotzinger, J.P., et al., 2005. Stratigraphy and sedimentology of a dry to wet eolian depositional system, Burns formation, Meridiani Planum, Mars. Earth Planet. Sci. Lett. 240, 11–72.

Hemingway, B.S., et al., 2002. Thermodynamic Data for Modeling Acid Mine Drainage Problems: Compilation and Estimation of Data for Selected Soluble Iron-Sulfate Minerals. United States Department of the Interior, U.S.G.S., pp. 1–13.

Iversen, N., Jørgensen, B.B., 1993. Diffusion coefficients of sulphate in marine sediments: influence of porosity. Geochim. Cosmochim. Acta 57, 571–578.

Kashkay, C.M., et al., 1975. Determination of DGf(298) of synthetic jarosite and its sulfate analogues. Geochem. Int. 12, 115–121.

Klingelhöfer, G., et al., 2004. Jarosite and hematite at Meridiani Planum from Opportunity's Mössbauer spectrometer. Science 306, 1740–1745.

Knauth, L.P., et al., 2005. Impact origin of sediments at the opportunity landing site on Mars. Nature 438, 1123–1128.

Knudson, A.T., et al., 2007. Aqueous geology in Valles Marineris: new insights in the relationship of hematite and sulfates from CRISM and HiRISE. Seventh International Conference on Mars.

Lane, M.D., et al., 2007. Identifying the Phosphate and Ferric Sulphate Minerals in the Paso Robles Soils (Gusev Crater, Mars) Using an Integrated Spectral Approach. Lunar Planet. Sci., XXXVIII. Lunar and Planetary Institute, Houston.

Lasaga, A.C., 1979. Treatment of multicomponent diffusion and ion-pairs in diagenetic fluxes. Am. J. Sci. 279, 324–346.

Lasaga, A.C., 1998. Kinetic Theory in the Earth Sciences. Princeton University Press, Princeton, New Jersey.

Li, Y.H., Gregory, S., 1974. Diffusion of ions in sea-water and in deep-sea sediments. Geochim. Cosmochim. Acta 38, 703–714.

Majzlan, J., et al., 2006. Formation, composition, structure, and ageing of As-ferrihydrite from Pezinok, Slovakia. Geochim. Cosmochim. Acta 70 (supplement), A385.

Marion, G.M., et al., 2003. Modeling aqueous ferrous iron chemistry at low temperatures with application to Mars. Geochim. Cosmochim. Acta 67, 4251–4266.

Marion, G.M., et al., 2008. Modeling ferrous–ferric iron chemistry with application to martian surface geochemistry. Geochemica et Cosmochimica Acta 72 (1), 242–266.

McLennan, S.M., et al., 2005. Provenance and diagenesis of the evaporite-bearing Burns formation, Meridiani Planum, Mars. Earth Planet. Sci. Lett. 240, 95–121.

Millero, F.J., Izaguirre, M., 1989. Effect of ionic-strength and ionic interactions on the oxidation of Fe(Ii). J. Solution Chem. 18, 585–599.

Morris, R.V., et al., 2005. Hematite spherules in basaltic tephra altered under aqueous, acid-sulfate conditions on Mauna Kea volcano, Hawaii: possible clues for the occurrence of hematite-rich spherules in the Burns formation at Meridiani Planum, Mars. Earth Planet. Sci. Lett. 240, 168–178.

Mozley, P.S., Davis, J.M., 2005. Internal structure and mode of growth of elongate calcite concretions: evidence for small-scale, microbially induced, chemical heterogeneity in groundwater. Geol. Soc. Amer. Bull. 117, 1400–1412.

Nordstrom, D.K., Munoz, J.L., 1994. Geochemical Thermodynamics. Blackwell Scienctific Publications.

Parker, V.B., Khodakovskii, I.L., 1995. Thermodynamic properties of the aqueous ions (2+ and 3+) of iron and the key compounds of iron. J. Phys. Chem. Ref. Data 24, 1699–1745.

Paterson, M.S., 1983. The equivalent channel model for permeability and resistivity in fluid-saturated rock — a re-appraisal. Mech. Mater. 345–352.

Peterson, R.C., Wang, R.Y., 2006. Crystal molds on Mars: melting of a possible new mineral species to create Martian chaotic terrain. Geology 34, 957–960.

Saar, M.O., Manga, M., 1999. Permeability–porosity relationship in vesicular basalts. Geophys. Res. Lett. 26, 111–114.

Schwertmann, U., Murad, E., 1983. Effect of Ph on the formation of goethite and hematite from ferrihydrite. Clays Clay Miner. 31, 277–284.

Sen, P.N., et al., 1981. A self-similar model for sedimentary rocks with application to the dielectric constant of fused glass beads. Geophysics 46, 781–795.

Squyres, S.W., Athena Science, T., 2004. Initial results from the MER Athena Science Team results at Gusev Crater and Meridiani Planum. Lunar Planet. Sci. Conf. XXXV (2187) (abstract).

Squyres, S.W., et al., 2004. In situ evidence for an ancient aqueous environment at Meridiani Planum, Mars. Science 306, 1709–1714.

Squyres, S.W., et al., 2006. Two years at Meridiani Planum: results from the Opportunity Rover. Science 313, 1403–1407.

Tosca, N.J., et al., 2005. Geochemical modeling of evaporation processes on Mars: insight from the sedimentary record at Meridiani Planum. Earth Planet. Sci. Lett. 240, 122–148.

Weitz, C.M., et al., 2006. Soil grain analyses at Meridiani Planum, Mars. J. Geophys. Res.-Planets 111, 1–26.

Wilkinson, M., 1991. "The rate of growth of sandstone-hosted calcite concretions": we have discovered an error in the paper by M. Wilkinson and M.D. Dampier, published in Geochimica et Cosmochimica Acta 54, 3391–3399. Geochim. Cosmochim. Acta 55, 1182.

Wilkinson, M., Dampier, M.D., 1990. The rate of growth of sandstone-hosted calcite concretions. Geochim. Cosmochim. Acta 54, 3391–3399.

Zahnle, K., Haberle, R.M., 2007. Atmospheric sulfur chemistry on ancient Mars. Seventh International Conference on Mars. Lunar and Planetary Institute, Pasadena, California.